Ultrafast spectroscopic investigation of discrete co-assemblies of a Zn-porphyrin–polymer conjugate with a hexapyridyl template

Wen-Dong Quan,[a] Lewis A. Baker,[b] Richard Napier,[c] Rachel K. O'Reilly,[d] Vasilios G. Stavros,[a] Michael Staniforth*[a] and Thomas R. Wilks*[d]

[a] Department of Chemistry, University of Warwick. Gibbet Hill Road, Coventry CV4 7AL, UK

[b] Faculty of Engineering and Physical Sciences, University of Surrey, 388 Stag Hill, Guildford GU2 7XH, UK

[c] School of Life Sciences, University of Warwick, Gibbet Hill Road, Coventry CV4 7AL, UK

[d] School of Chemistry, University of Birmingham, Edgbaston, Birmingham B15 2TT, UK

* Corresponding author email addresses: m.staniforth@warwick.ac.uk; t.r.wilks@bham.ac.uk

Abstract

One of the key features of biological light harvesting complexes (LHCs) is their incorporation of multi-chromophoric reaction centres via non-covalent interactions. Most synthetic mimics require relatively complex syntheses and are constructed in organic solvents. Here, we report the use of polymer self-assembly to enable the formation of Zn-porphyrin–pyridine complexes in aqueous solution. We show that self-assembly opens up new photophysical relaxation pathways, measured through time-resolved femtosecond pump-probe spectroscopy, suggesting that it may be a useful additional strategy for the construction of more advanced LHC mimics.

Introduction

Photosynthesis is one of the most important biochemical processes on Earth. Plants and photosynthetic microorganisms achieve the extraordinary photochemical energy conversion efficiencies required via their light harvesting complexes (LHCs).[1–15] Biophysical research over the past few decades has revealed two of the biological LHCs' key 'trade secrets': i) their abilities to trap and channel light energy into the reaction centres on ultrafast time scales;[1–4,10–15] attributed to ii) the precise, yet minimalist arrangement of light absorbing pigments, achieved through an assortment of naturally-occurring supramolecular interactions.[5–7] These, in turn, have provided the blueprint for numerous attempts to create synthetic mimics of multi-chromophoric arrays. Such arrays are predominantly achieved by arranging porphyrin variants, highly versatile synthetic forms of biological pigments (chlorophylls), by two main methods.[16–19] The first is by direct conjugation of chromophores, typically into *n*-chromophore oligomers/polymers (*n*>5), producing robust and well defined nanoarrays, especially in the presence of templates.[20–25] The second is by the binding of multiple smaller fragments of up to 3 chromophores via intermolecular interactions, typically metal-ligand. The latter may be considered closer mimics of biological systems but are more susceptible to disruption from their solvent environment.[16,19] These methods all produce elegant arrays of chromophores capable of intermolecular and intramolecular electronic energy transfer (EET),[26–28] but complementary approaches would broaden the scope of LHC mimics even further.

One such approach is the self-assembly of porphyrin-containing amphiphilic copolymers.[29] By incorporation either at the chain end or as a linker between polymer blocks, a wide variety of structures have been synthesised that exploit the catalytic, fluorescent or therapeutic properties of porphyrin derivatives.[30–35] Typically, however, these rely on porphyrin–porphyrin interactions alone for the modulation of photophysical behaviour. Here, we report the co-assembly of an amphiphilic polymer–porphyrin conjugate with a multidentate template in water. Nanoscale

assemblies were observed, and photophysical studies suggested that new photophysical pathways were opened as a result of template incorporation. This study illustrates the potential of solution self-assembly as an alternative method for the construction of complex LHC mimics.

Results and Discussion

Our previous work on the aqueous self-assembly of amphiphilic polymer–porphyrin conjugates has demonstrated that the photophysical behaviour of the free porphyrin can be preserved in a nanoscale assembly.[36] We therefore used this previously reported system as a starting point for the present work. A dialkyne-functionalised Zn diphenylporphyrin (**Zn-dPP**) was functionalised with the water soluble polymer poly(dimethylacrylamide) (**PDMA**) via copper-catalysed azide–alkyne cycloaddition as previously described,[36] to give **Zn-dPP-PDMA** (Figure 1a). We then explored co-assembly of this polymer–porphyrin conjugate with a LHC reaction centre mimic. A hexapyridyl benzene derivative (**T-pyr**, Figure 1a) was chosen for this purpose because its interactions with porphyrins have been extensively characterised by Anderson and coworkers.[25] Although **T-pyr** has been shown to bind six porphyrins by Zn···N coordination[25] we reasoned that the presence of bulky polymer arms may have altered the preferred stoichiometry. Co-assembly of **Zn-dPP-PDMA** and **T-pyr** was therefore attempted at different porphyrin:pyridine molar ratios (Figure 1a). Appropriate quantities of **Zn-dPP-PDMA** and **T-pyr** were dissolved in tetrahydrofuran (THF) by sonication for 15-30 minutes. An equal volume of 18.2 MΩ cm water was then added slowly using a peristaltic pump, and the mixture dialysed against 18.2 MΩ cm water to remove THF using a 3.5 kDa molecular weight cut-off membrane. The samples were then analysed by steady-state ultraviolet-visible (UV-vis) spectroscopy. Zn···N coordination was expected to manifest as a red-shift of 10-20 nm in the Soret band (400-450 nm) in line with previous reports.[37–40] Interestingly, no red-shift was observed at a pyridine:porphyrin ratio of 1:1 (Figure 1b), in contrast with previous reports on porphyrin nanorings.[37,38] Indeed, a pyridine:porphyrin ratio of 6:1 was necessary for a significant red-shift to be observed. Because each template molecule

contained six pyridine sites, this meant that, on average, each template **T-pyr** was bound to a single **Zn-dPP-PDMA**. Increasing the ratio beyond this did not lead to any further changes in the UV-vis spectrum, from which we inferred that Zn···N coordination had already been maximized. We speculate that the increased amount of pyridine required for effective Zn···N coordination may be due in part to competition from the triazole rings in **Zn-dPP-PDMA**, which have previously been shown to coordinate Zn and drive assembly behaviour in a polymer-based system.[36,41] It is important to note that no change in the shift of the Soret band was observed for the self-assembly of **Zn-dPP-PDMA**, confirming that the red-shift observed for the porphyrin:pyridine complex was not due to either porphyrin aggregation or triazole-porphyrin interactions alone. Additionally, no shift in the Q-band was observed for these samples.

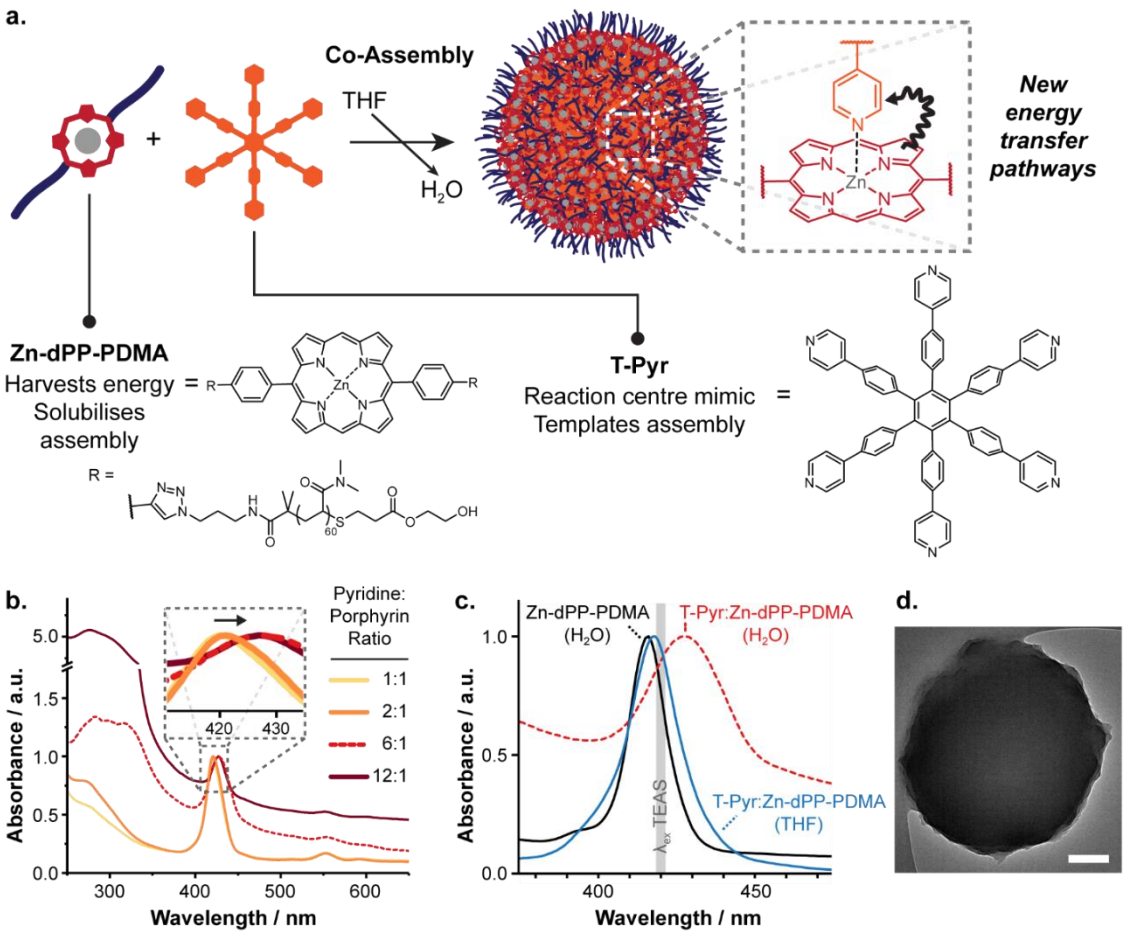

Figure 1. *Co-assembly of a porphyrin-polymer conjugate (**Zn-dPP-PDMA**) with a multidentate template (**T-Pyr**) to generate nanoparticles in water. a) Schematic of the self-assembly process showing the structures of **Zn-dPP-PDMA** and **T-Pyr**, with one plausible new pathway indicated. b) UV-vis absorption spectra of **T-pyr···Zn-dPP-PDMA** assembled in water at different pyridine:porphyrin ratios, showing the shift in the Soret band due to Zn···N coordination. c) UV-Vis absorption spectra of **T-pyr···Zn-dPP-PDMA** solvated in THF (blue), **T-pyr···Zn-dPP-PDMA** assembled in water (red, dashed) and **Zn-dPP-PDMA** assembled in water (black), showing the shift in the Soret band in the presence of the template, **T-Pyr**. d) Dry state TEM image of one of the self-assembled nanoparticles, imaged on graphene oxide without staining; scale bar = 200 nm.*

We proceeded to further analyse the self-assemblies obtained at the optimised pyridine:porphyrin ratio of 6:1, which, for the sake of brevity, we refer to as **T-pyr···Zn-dPP-PDMA**. The steady-state UV-vis spectrum of the **T-pyr···Zn-dPP-PDMA** self-assembly in water was compared with that for

a self-assembly of **Zn-dPP-PDMA** alone (Figure 1c). This further highlighted the expected red-shift in the Soret band as a result of Zn···N coordination, as well as an increase in baseline absorbance, which we attribute to scattering by the large self-assembled particles. The spectrum of a mixture of **T-pyr** and **Zn-dPP-PDMA** was also recorded in THF. Both components were freely soluble in this solvent, so it was expected that no self-assembly would occur: as anticipated, no significant red-shift was observed, consistent with the absence of Zn···N coordination. The spectrum of **T-pyr** alone was also recorded in THF at the same concentration. This showed the characteristic absorption peak of the aromatic system around 280 nm (see SI, Figure S1). The spectrum of the **T-pyr···Zn-dPP-PDMA** self-assembly in water also showed increased absorption at 320 nm, not present in either of the individual systems alone (see Figure 1b and Figure S1), which was consistent with the formation of new interactions between the two components. Finally, it was observed that **T-Pyr** alone was insoluble in water, even when a slow solvent switch from THF (a good solvent) to water was attempted. Taken together, these results strongly imply that co-assembly of **T-pyr···Zn-dPP-PDMA** in water driven by Zn···N coordination was occurring, and that the photophysical properties had been altered significantly. Inspection of **T-pyr···Zn-dPP-PDMA** by dry state transmission electron microscopy confirmed the presence of large, irregular self-assembled structures (Figure 1d).

The photophysics of the system were investigated in greater detail using transient electronic absorption spectroscopy (TEAS, see SI for further details). Samples were excited at 420 nm, a compromise between the absorption maxima of the aqueous self-assemblies of **Zn-dPP-PDMA** and **T-pyr···Zn-dPP-PDMA**, but exciting within the Soret band in both cases (cf. Figure 1c). We did not investigate excitation within the Q-band, which could be the subject of future work. **T-pyr** alone was not studied as it did not significantly absorb wavelengths longer than around 350 nm (Figure S1), nor was it soluble in water without the presence of **Zn-dPP-PDMA**. False colour heat maps of the transient electronic absorption spectra for **Zn-dPP-PDMA** solvated

in THF, and **T-pyr···Zn-dPP-PDMA** solvated in THF and assembled in water, along with spectra at specific pump-probe time-delays, Δ*t*, are presented in Figure 2a-f. In these spectra, the change in absorption (ΔmOD) relative to the ground state is plotted as a function of time, up to a maximum pump-probe time delay of 2 ns. In all cases, upon photoexcitation, a ground state bleach (GSB) in the Soret band (ca. 416 nm) and two excited state absorption (ESA) shoulders, <400 nm and between 450-550 nm, were observed. As expected, the GSB in the aqueous assembly of **T-pyr···Zn-dPP-PDMA** was red-shifted compared to the same mixture dissolved in THF (in accordance with the steady-state UV-Vis measurements in Figure 1c, see Figure S2). Notably, ~75% GSB recovery was observed for the aqueous sample, in stark contrast to the sample in THF where the GSB persisted well beyond 2 ns.[39]

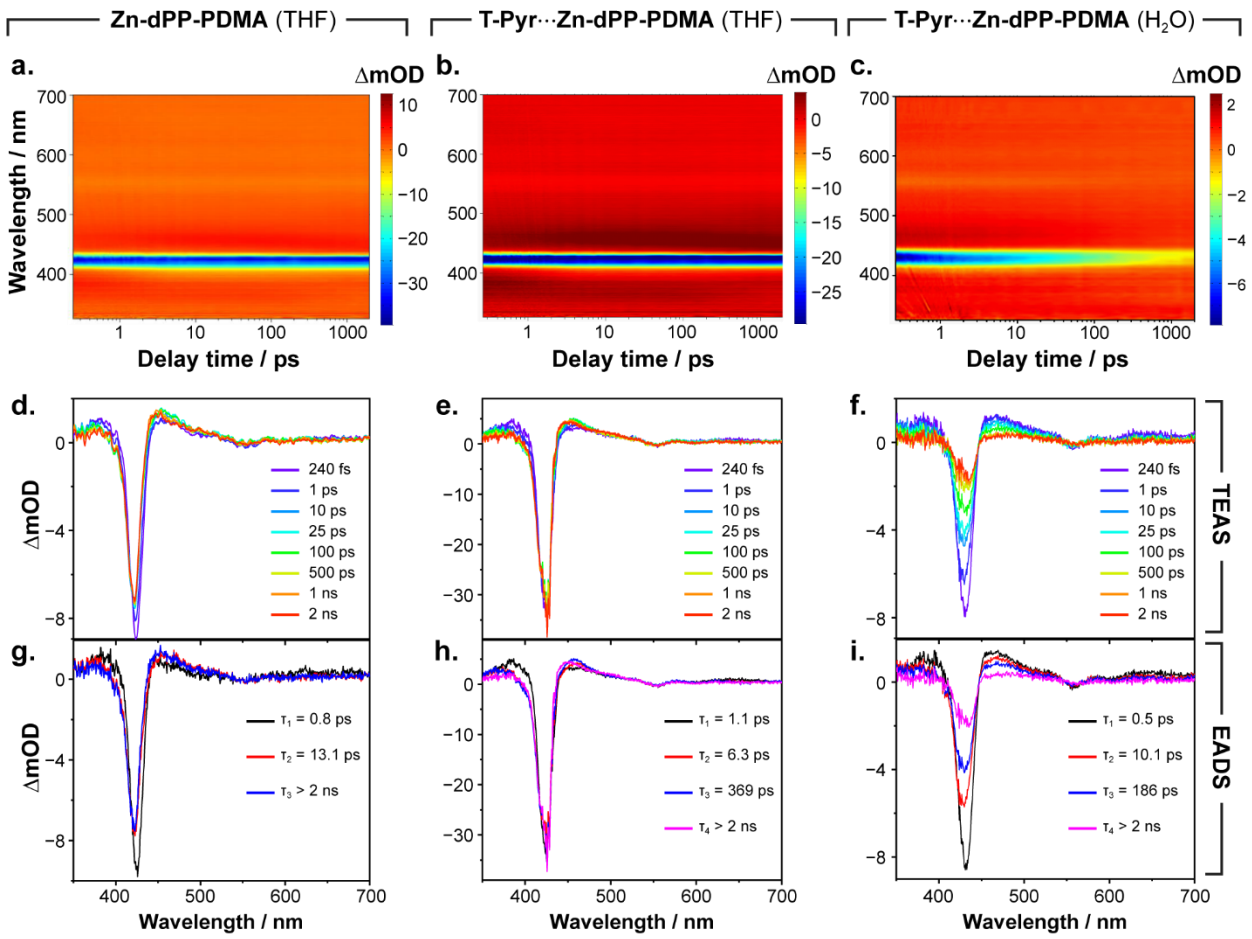

Figure 2. *Investigation of photophysics via TEAS at 420 nm excitation for* ***Zn-dPP-PDMA*** *alone (left hand column) and* ***T-pyr···Zn-dPP-PDMA*** *in THF (middle column) and water (right hand column). a-c) False colour heat maps of the transient electronic absorption spectra. d-f) Selected transient electronic absorption spectra at indicated pump/probe time delays. g-i) Evolution-associated difference spectra for the extracted time constants.*

To begin to understand the underlying dynamics, the collected spectra were investigated with a global fitting sequential kinetic model in the Glotaran software package.[42] For **Zn-dPP-PDMA** alone solvated in THF, three distinct processes with associated lifetimes (Table 1) were required to reconstruct the collected spectra (cf. residual fits in Figure S3). These lifetimes agreed well with previous data on the same system in dioxane when excited at 400 nm,[36] demonstrating that the change in both non-polar solvent and excitation wavelength had little to no effect on the observed

dynamics. By contrast, for **T-pyr···Zn-dPP-PDMA** samples (with THF or water as the solvent), four processes with associated lifetimes (Table 1) were required to reconstruct the collected spectra. Three of these processes (with lifetimes τ_1, τ_2 and τ_4) approximated those observed for **Zn-dPP-PDMA** alone. The newly observed processes (with time constants τ_3) varied depending on the solvent (369 ps in THF compared with 186 ps in water).

Table 1. *Extracted lifetimes from global fit analysis of TEAS data.*

System (solvent, excitation wavelength)	**Lifetime / ps**			
	τ_1	**τ_2**	**τ_3**	**τ_4**
Zn-dPP-PDMA (Dioxane, 400 nm)[39]	1.0±0.3	20.3±8	>2000	-
Zn-dPP-PDMA (H_2O, 400 nm)[39]	0.8 ±0.3	15.2±6	>2000	-
Zn-dPP-PDMA (THF, 420 nm)	0.8±0.04	13.1±1.6	>2000	-
T-pyr···Zn-dPP-PDMA (THF, 420 nm)	1.1±0.06	6.3±0.5	369±30	>2000
T-pyr···Zn-dPP-PDMA (H_2O, 420 nm)	0.46±0.04	10.1±0.7	186±12	>2000

To give further insight into the excited state species involved, evolution-associated difference spectra (EADS) were calculated for the extracted lifetimes in each sample, using a sequential model (Figure 2g-i). EADS estimate what the transient electronic absorption spectra would look like were it possible to observe each excited state species on its own, and are therefore useful in picking out similarities and differences between the systems under study. The EADS for τ_1, τ_2, and τ_4 for **T-pyr···Zn-dPP-PDMA** in THF closely resembled those for τ_1, τ_2 and τ_3 respectively for **Zn-dPP-PDMA** alone in THF, indicating no significant differences between the excited state

species involved in the dynamics of these two systems. The origin of the additional time constant for **T-pyr···Zn-dPP-PDMA** in THF was uncertain, but the similarity of its EADS to those for the other time constants indicated that it was likely associated with a similar dynamic process to that observed for **Zn-dPP-PDMA** alone. The origin of τ_3 in **T-pyr···Zn-dPP-PDMA** is discussed in more detail below.

The EADS for **T-pyr···Zn-dPP-PDMA** in water differed significantly from those in THF; notably, the negative peak due to the GSB steadily decreased in intensity for each successive time constant. These data imply that multiple different decay pathways became available to **T-pyr···Zn-dPP-PDMA** as a result of self-assembly in water. The presence of a persistent GSB for τ_4 suggested that a proportion (<25%) of the initial excited state still resulted in populating a long-lived excited state, despite competition from the newly introduced decay pathways. The contribution to the dynamics of GSB recovery in each time constant is highly unusual and worth further discussion. It would normally be the case that a process causing the system to return to the ground state in ~1 ps would vastly outcompete those taking orders of magnitude longer (such as τ_3 and τ_4). The fact that this does not seem to be the case here, and indeed, each dynamical pathway observed appears to occur in competition with ground state recovery, suggests that the photophysics of the **T-pyr···Zn-dPP-PDMA** assembly are particularly complex.

Quantum mechanical calculations were performed to help identify the molecular orbitals most likely to be involved in the dynamics of **T-pyr···Zn-dPP-PDMA** in water. To make the calculations tractable, only dimers of a single porphyrin, coupled with a single template, were studied. Calculations were performed using the Turbomole[43,44] software package, using density functional theory, with the B-P86 functional,[45,46] the def2-SV(P) basis set,[47] the 'M4' quadrature scheme,[48] and employing the resolution of identity and multipole accelerated resolution of identify approximations with default auxiliary basis sets.[49,50] The molecular orbitals associated with the Soret band transition were calculated – those with significant oscillator strength in the region of

the Soret band are listed in Table 2. The results revealed two transitions with similar oscillator strengths, at 446 and 447 nm, originating from an orbital localised around the porphyrin (Figure 3, orbital 624) and finishing on one located on the template (Figure 3, orbital 637). Although the situation in the self-assembled system will be much more complex, these calculations provide qualitative evidence that **T-pyr···Zn-dPP-PDMA** complexation leads to the introduction of transitions that involve both the porphyrin and the template. It is possible that these transitions involve charge transfer, but further investigations would be required to confirm the exact nature of the process.

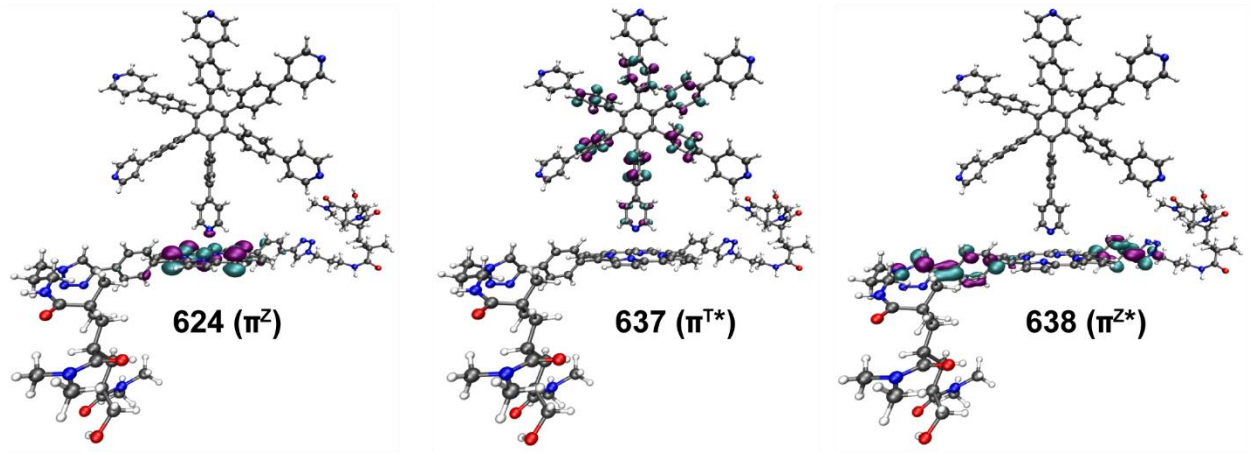

Figure 3. *Representations of the calculated molecular orbitals involved in the Soret band transition of the* ***T-pyr···Zn-dPP-PDMA*** *co-ordinated complexes. The orbital numbers and names correspond to those listed in Table 2. Superscript letters denote whether the orbital resides mainly on the Zn porphyrin (Z) or the template (T). Excited states are indicated with a *.*

Table 2. *Details of calculated molecular orbitals with significant oscillator strength in the region of the Soret band. As above, superscript letters denote whether the orbital resides mainly on the Zn porphyrin (Z) or the template (T). Excited states are indicated with a *.*

Calculated transition wavelength / nm	Molecular orbital contribution and character			
	Initial orbital	Final orbital	Contribution	Oscillator strength
447	624 (π^Z)	637 (π^T*)	60%	0.3
	624 (π^Z)	638 (π^Z*)	30%	
446	624 (π^Z)	637 (π^T*)	30%	0.2
	624 (π^Z)	638 (π^Z*)	60%	

The dynamics of **Zn-dPP-PDMA** have been previously explored and are attributed to i) ultrafast internal conversion from the photoexcited S_2 (Soret) state to the lower lying S_1 state, followed by ii) intermolecular vibrational energy transfer (IET) from the solvent to the solute and iii) a long lived population of the S_1 state, which undergoes intersystem crossing (ISC) to a triplet state on a timescale beyond the limit of our experiments.[36] In this previous work, **Zn-dPP-PDMA** was studied in dioxane and H_2O at 400 nm (*cf* present work in H_2O and THF at 420 nm). However, the strong similarities with the data reported here suggest that the same process operates for **Zn-dPP-PDMA** when excited at 420 nm in THF. We postulate that upon addition of **T-pyr** the same S_2 excited state is accessed. This is evidenced by the strong similarity in EADS for τ_1, as outlined above. The reduced lifetime of τ_2 as well as the additional lifetime observed (τ_3 ~369 ps), however, suggest that the IET cooling process on the S_1 energy surface is more complicated when the template is present. It is possible that vibrational coupling between dimers of **Zn-dPP-PDMA** and **T-pyr** decreases the lifetime of τ_2, with τ_3 representing the relaxation of a small proportion of **T-pyr** excited by this energy transfer. However, the small amplitude in the changes between the different EADS for τ_2, τ_3, and τ_4 make precise determination of these dynamics very challenging.

Importantly, the similarity in the EADS for τ_4, though, confirm that the majority of the photoexcited population ends up in the same long-lived S_1 state.

For **T-pyr···Zn-dPP-PDMA** in water, our computational study suggests that, upon assembly, new transitions involving both the template and the porphyrin become accessible. It is likely that these play a significant role in the relaxation dynamics of the assembly although, once again, the precise mechanism is difficult to discern for a number of reasons: i) the simplicity of the model used, necessary to make the calculations tractable; and ii) the complexity of the dynamics observed. It would normally be the case that, should there be a competitive pathway to the ground state of the assembly, it would dominate the dynamics. However, in this case, each of the EADS showed significant ground state recovery, suggesting multiple parallel pathways back to the original ground state of the system, all of which are competitive with one another (see above). The global fitting sequential kinetic model is thus a simplification of the dynamics. Further insight into the identity of these parallel pathways would be needed before a complete kinetic model could be constructed and used to fit the collected spectra, something which is beyond the scope of this current work.

Bringing these observations together, we propose that co-assembly of **T-pyr···Zn-dPP-PDMA** in water results in a number of new transitions becoming accessible, which enable some of the initial S_2 excited state population to be funneled back to the electronic ground state, S_0. Repopulation of the ground state then continues to occur at every stage of the relaxation process. A proportion (<25%) of the initial excited state still ends up populating the long-lived S_1 excited state, which undergoes ISC on a timescale beyond the window of our measurements, giving rise to the long-lived GSB signal observed in τ_4. These results clearly highlight the potential of polymer self-assembly for the creation of multichromophore arrays, which may in the future be capable of mimicking the light harvesting complexes found in nature.

Conclusion

In summary, we have demonstrated the construction of a multichromophore array, without the need for direct inter-chromophoric conjugation. The experimental observations suggest that new photophysical relaxation pathways for the chromophores were introduced by assembling the system in the presence of an N-donor ligand. More importantly, these additional relaxation pathways were only observed upon assembly, not when the chromophores were fully solvated with identical concentrations, suggesting that **T-pyr···Zn-dPP-PDMA** coordination is likely 'switched on' by the dense packing induced by self-assembly. Further work is needed to elucidate the nature of the excited state species involved, for example through fluorescence decay or electrochemical measurements, which will in turn enable a quantitative understanding of the relation processes involved. Nevertheless, we posit that this method could be a viable strategy for creating similar functionally-enhanced complexes for other biomimetic systems. The lack of direct covalent conjugation between the chromophores required also reduces the complexity of the syntheses involved. Thus, we propose that the present method could be an attractive alternative for large-scale production of multi-chromophoric nanostructures. In conjunction with the continual improvement in hexaarylbenzene synthetic methods, we hope that this work could improve the accessibility of future biomimetic light harvesting systems.

Acknowledgements

WDQ was supported by a studentship from the Molecular Assembly and Organisation in Cells Centre for Doctoral Training at the University of Warwick. VGS and MS thank the EPSRC for equipment grant EP/J007153; and VGS the Royal Society and the Leverhulme Trust for a Royal Society Leverhulme Trust Senior Research Fellowship. RKO and TRW thank the University of Birmingham for funding. The authors are grateful for computational resources provided by Scientific Computing Research Technology Platform at the University of Warwick.

Keywords: Self-assembly, Polymer, Porphyrin, LHC mimic, Supramolecular, Photophysics, Transient absorption.

References

1 B. F. Milne, C. Kjær, J. Houmøller, M. H. Stockett, Y. Toker, A. Rubio and S. B. Nielsen, *Angew. Chem. Int. Ed.*, 2016, **55**, 6248–6251.

2 X. Qin, M. Suga, T. Kuang and J.-R. Shen, *Science*, 2015, **348**, 989–995.

3 E. Collini, C. Y. Wong, K. E. Wilk, P. M. G. Curmi, P. Brumer and G. D. Scholes, *Nature*, 2010, **463**, 644–647.

4 G. Trinkunas, J. L. Herek, T. Polívka, V. Sundström and T. Pullerits, *Phys. Rev. Lett.*, 2001, **86**, 4167–4170.

5 M. Suga, F. Akita, K. Hirata, G. Ueno, H. Murakami, Y. Nakajima, T. Shimizu, K. Yamashita, M. Yamamoto, H. Ago and J.-R. Shen, *Nature*, 2015, **517**, 99–103.

6 Y. Umena, K. Kawakami, J.-R. Shen and N. Kamiya, *Nature*, 2011, **473**, 55–60.

7 L. Dall'Osto, M. Bressan and R. Bassi, *Biochim. Biophys. Acta - Bioenerg.*, 2015, **1847**, 861–871.

8 Z. Yang, W. Qin, N. L. C. Leung, M. Arseneault, J. W. Y. Lam, G. Liang, H. H. Y. Sung, I. D. Williams and B. Z. Tang, *J. Mater. Chem. C*, 2015, **4**, 99–107.

9 J. M. Anna, G. D. Scholes and R. van Grondelle, *Bioscience*, 2014, **64**, 14–25.

10 R. Moca, S. R. Meech and I. A. Heisler, *J. Phys. Chem. B*, 2015, **119**, 8623–8630.

11 D. I. G. Bennett, K. Amarnath and G. R. Fleming, *J. Am. Chem. Soc.*, 2013, **135**, 9164–9173.

12 H. Liu, H. Zhang, D. M. Niedzwiedzki, M. Prado, G. He, M. L. Gross and R. E. Blankenship,

Science, 2013, **342**, 1104–1107.

13 G. S. Schlau-Cohen, J. M. Dawlaty and G. R. Fleming, *IEEE J. Sel. Top. Quantum Electron.*, 2012, **18**, 283–295.

14 M. Ballottari, M. J. P. Alcocer, C. D'Andrea, D. Viola, T. K. Ahn, A. Petrozza, D. Polli, G. R. Fleming, G. Cerullo and R. Bassi, *Proc. Natl. Acad. Sci.*, 2014, **111**, E2431–E2438.

15 G. S. Engel, T. R. Calhoun, E. L. Read, T.-K. Ahn, T. Mančal, Y.-C. Cheng, R. E. Blankenship and G. R. Fleming, *Nature*, 2007, **446**, 782–786.

16 N. Aratani, D. Kim and A. Osuka, *Acc. Chem. Res.*, 2009, **42**, 1922–1934.

17 F. Durola, V. Heitz, F. Reviriego, C. Roche, J.-P. Sauvage, A. Sour and Y. Trolez, *Acc. Chem. Res.*, 2014, **47**, 633–645.

18 Q. Yan, Z. Luo, K. Cai, Y. Ma and D. Zhao, *Chem. Soc. Rev.*, 2014, **43**, 4199–4221.

19 Y. Nakamura, N. Aratani and A. Osuka, *Chem. Soc. Rev.*, 2007, **36**, 831–845.

20 S.-P. Wang, Y.-F. Shen, B.-Y. Zhu, J. Wu and S. Li, *Chem. Commun.*, 2016, **52**, 10205–10216.

21 M. C. O'Sullivan, J. K. Sprafke, D. V Kondratuk, C. Rinfray, T. D. W. Claridge, A. Saywell, M. O. Blunt, J. N. O'Shea, P. H. Beton, M. Malfois and H. L. Anderson, *Nature*, 2011, **469**, 72–75.

22 J. K. Sprafke, B. Odell, T. D. W. Claridge and H. L. Anderson, *Angew. Chem. Int. Ed.*, 2011, **50**, 5572–5575.

23 S. Liu, D. V Kondratuk, S. A. L. Rousseaux, G. Gil-Ramírez, M. C. O'Sullivan, J. Cremers, T. D. W. Claridge and H. L. Anderson, *Angew. Chem. Int. Ed.*, 2015, **54**, 5355–5359.

24 D. V Kondratuk, L. M. A. Perdigão, A. M. S. Esmail, J. N. O'Shea, P. H. Beton and H. L.

Anderson, *Nat. Chem.*, 2015, **7**, 317–322.

25 M. Hoffmann, J. Kärnbratt, M.-H. Chang, L. M. Herz, B. Albinsson and H. L. Anderson, *Angew. Chem. Int. Ed.*, 2008, **47**, 4993–4996.

26 P. Parkinson, N. Kamonsutthipaijit, H. L. Anderson and L. M. Herz, *ACS Nano*, 2016, **10**, 5933–5940.

27 A. Mikhaylov, D. V Kondratuk, A. Cnossen, H. L. Anderson, M. Drobizhev and A. Rebane, *J. Phys. Chem. C*, 2016, **120**, 11663–11670.

28 S. Fukuzumi, T. Honda and T. Kojima, *Coord. Chem. Rev.*, 2012, **256**, 2488–2502.

29 J. Tian and W. Zhang, *Prog. Polym. Sci.*, 2019, **95**, 65–117.

30 E. Huynh, B. Y. C. Leung, B. L. Helfield, M. Shakiba, J.-A. Gandier, C. S. Jin, E. R. Master, B. C. Wilson, D. E. Goertz and G. Zheng, *Nat. Nanotechnol.*, 2015, **10**, 325–332.

31 T. V Duncan, P. P. Ghoroghchian, I. V Rubtsov, D. A. Hammer and M. J. Therien, *J. Am. Chem. Soc.*, 2008, **130**, 9773–9784.

32 Y. Liu, S. Li, K. Li, Y. Zheng, M. Zhang, C. Cai, C. Yu, Y. Zhou and D. Yan, *Chem. Commun.*, 2016, **52**, 9394–9397.

33 L. Xu, L. Liu, F. Liu, H. Cai and W. Zhang, *Polym. Chem.*, 2015, **6**, 2945–2954.

34 J. Lu, L. Liang and M. Weck, *J. Mol. Catal. A Chem.*, 2016, **417**, 122–125.

35 J. F. Lovell, C. S. Jin, E. Huynh, H. Jin, C. Kim, J. L. Rubinstein, W. C. W. Chan, W. Cao, L. V Wang and G. Zheng, *Nat. Mater.*, 2011, **10**, 324–332.

36 W.-D. Quan, A. Pitto-Barry, L. A. Baker, E. Stulz, R. Napier, R. K. O'Reilly and V. G. Stavros, *Chem. Commun.*, 2016, **52**, 1938–1941.

37 J.-X. Zhang, F.-M. Han, J.-C. Liu, R.-Z. Li and N.-Z. Jin, *Tetrahedron Lett.*, 2016, **57**, 1867–

1872.

38 E. M. Finnigan, R. Rein, N. Solladié, K. Dahms, D. C. G. Götz, G. Bringmann and M. O. Senge, *Tetrahedron*, 2011, **67**, 1126–1134.

39 C. C. Mak, N. Bampos and J. K. M. Sanders, *Angew. Chem. Int. Ed.*, 1998, **37**, 3020–3023.

40 C. A. Hunter, M. N. Meah and J. K. M. Sanders, *J. Am. Chem. Soc.*, 1990, **112**, 5773–5780.

41 D. A. Roberts, T. W. Schmidt, M. J. Crossley and S. Perrier, *Chem. – A Eur. J.*, 2013, **19**, 12759–12770.

42 J. J. Snellenburg, S. Laptenok, R. Seger, K. M. Mullen and I. H. M. van Stokkum, *J. Stat. Softw.*, 2012, **1**, 1–22.

43 M. Von Arnim and R. Ahlrichs, *J. Comput. Chem.*, 1998, **19**, 1746–1757.

44 R. Ahlrichs, M. Bär, M. Häser, H. Horn and C. Kölmel, *Chem. Phys. Lett.*, 1989, **162**, 165–169.

45 A. D. Becke, *Phys. Rev. A*, 1988, **38**, 3098–3100.

46 J. P. Perdew, *Phys. Rev. B*, 1986, **33**, 8822–8824.

47 F. Weigend and R. Ahlrichs, *Phys. Chem. Chem. Phys.*, 2005, **7**, 3297–3305.

48 O. Treutler and R. Ahlrichs, *J. Chem. Phys.*, 1995, **102**, 346–354.

49 H. Eshuis, J. Yarkony and F. Furche, *J. Chem. Phys.*, 2010, **132**, 234114.

50 M. Sierka, A. Hogekamp and R. Ahlrichs, *J. Chem. Phys.*, 2003, **118**, 9136–9148.

Supplementary Information

for

Enhanced formation of Zn-porphyrin charge transfer complexes driven by polymer self-assembly

Wen-Dong Quan,[a] Lewis A. Baker,[b] Richard Napier,[c] Rachel K. O'Reilly[d],

Vasilios G. Stavros[a], Michael Staniforth[a*], and Thomas R. Wilks[d*]

[a] Department of Chemistry, University of Warwick, Gibbet Hill Road, Coventry, UK

[b] Faculty of Engineering and Physical Sciences, University of Surrey, 388 Stag Hill, Guildford, GU2 7XH, UK

[c] School of Life Sciences, University of Warwick, Gibbet Hill Road, Coventry, UK

[d] School of Chemistry, University of Birmingham, Edgbaston, Birmingham, UK

* m.staniforth@warwick.ac.uk; t.r.wilks@bham.ac.uk

Synthetic Methods

Spectroscopic grade tetrahydrofuran (THF) was purchased from VWR. Water for synthesis and spectroscopy was purified to a resistivity of 18.2 MΩ cm using a Millipore Simplicity Ultrapure water system. All other solvents and chemicals were purchased from Sigma, Aldrich, Fluka or Acros and used as received. Zn-5,15-bis(4-ethynylphenyl)-porphyrin (**Zn-dPP**), Zn-

diphenylporphyrin-poly-*N*,*N*-dimethylacrylamide (**Zn-dPP-PDMA**)[1] and the hexadentate template (**T-pyr**)[2] were synthesised according to reported methods.

Co-Assembly of T-Pyr and Zn-dPP-PDMA

T-Pyr and **Zn-dPP-PDMA** were dissolved in tetrahydrofuran and sonicated for 15-30 minutes to ensure complete dissolution. An equal volume of water was then added dropwise by peristaltic pump with stirring. The resulting mixture was dialysed against a large excess of 18.2 MΩ cm water using dialysis tubing with a 3.5 kDa molecular weight cut-off. A minimum of four water changes were performed to ensure complete removal of the THF cosolvent. Small scale tests were performed to ascertain the optimum pyridine:porphyrin ratio, using 4.5 mg of **Zn-dPP-PDMA**, the appropriate mass of **T-Pyr** and 1.5 mL of THF. For the optimised ratio of 6:1 pyridine:porphyrin, a larger scale assembly was performed to provide sufficient sample volume for further characterisation, using 45 mg of **Zn-dPP-PDMA**, 3 mg of **T-Pyr** and 15 mL of THF.

Transmission Electron Microscopy (TEM)

Dry-state transmission electron microscopy (TEM) samples were prepared on graphene oxide (GO)-coated carbon grids (Quantifoil R2/2).[3] Generally, 20 µL of sample was pipetted on a grid, blotted immediately and left to air dry prior to observation.

UV-Vis Absorption and Transient Electronic Absorption Spectroscopy

Steady-state ultraviolet-visible (UV-Vis) spectroscopy was carried out on an Agilent Cary 60 UV-Vis spectrometer. Quartz cells with screw caps and four polished sides (Starna) were used for UV-Vis measurements. The detailed experimental procedures for transient electronic absorption spectroscopy (TEAS) can be found in previous reports.[1,4] Briefly, a commercially available Ti:sapphire oscillator and amplifier system (Spectra-Physics) produces 3 mJ laser pulses of ~40 fs duration centred around 800 nm with a repetition rate of 1 kHz. For TEAS, pump pulses (λpu) were generated from the 800 nm fundamental using a Spectra-Physics TOPAS-C optical

parametric amplifier, to produce λpu of 420 nm with powers of between 0.3-0.5 mW and a pulse duration of 80 fs. 5% of a 1 mJ/pulse 800 nm laser beam (50 μJ/pulse) is focused onto a CaF_2 window to generate the probe pulse, a white light continuum (330-725 nm). Pump/probe polarizations are held at the magic angle (54.7°) relative to one another. Changes in optical density (ΔOD) of the sample are calculated from probe intensities, collected using a spectrometer (Avantes, AvaSpec-ULS1650F) using the following equation:

$$\Delta OD = -log\left(\frac{I(\lambda)_{pu}}{I(\lambda)_{un}}\right) \quad (1)$$

Here $I(\lambda)_{un}$ is the wavelength dependent intensity of the transmitted light through the unpumped sample and $I(\lambda)_{pu}$ is the wavelength dependent intensity of transmitted light through the pumped sample. A delay stage is positioned in the probe path which introduces a time delay Δ*t*, between the arrival of the probe pulses relative to pump pulses, up to a maximum of Δ*t* = 2 ns. The delivery system for the samples is a flow-through cell (Demountable Liquid Cell by Harrick Scientific Products, Inc.). The sample is circulated using a peristaltic pump (Masterflex) with PTFE tubing, recirculating sample from a 50 mL reservoir (with minimum sample volume of *ca*. 20 mL), in order to provide each pump-probe pulse pair with fresh sample. All resultant transient electronic absorption (TEA) spectra were chirp-corrected using the KOALA package.[5]

Analysis of TEAS data: Global fitting and Evolution Associated Decay Spectra

Analysis of TEAS data was performed by means of globally fitting the data to a number of exponential decay lifetimes using the Glotaran software package.[6] Each lifetime correlates to an evolution associated difference spectrum (EADS). These spectra are a measure of the difference in absorption of the populated species relative to the unpumped ground state, which decays into the next species with the lifetime associated with that EADS. Thus, each EADS will generally consist of a number of components including: the ground state bleach (GSB), a negative signal caused by the loss of population of the ground state; excited state absorptions (ESA),

positive signals caused by absorption of light by the newly formed excited state or states; stimulated emission (SE), a negative signal caused by emission of light from an excited state, stimulated by the probe pulse; and the positive absorption of any photoproducts that might be present. The EADS therefore gives information on where the excited population resides for each step of the dynamics, and the lifetime of those states or photoproducts, as well as information on the recovery of the GSB as population funnels back to the original ground state.

Steady-State UV-Visible Spectra

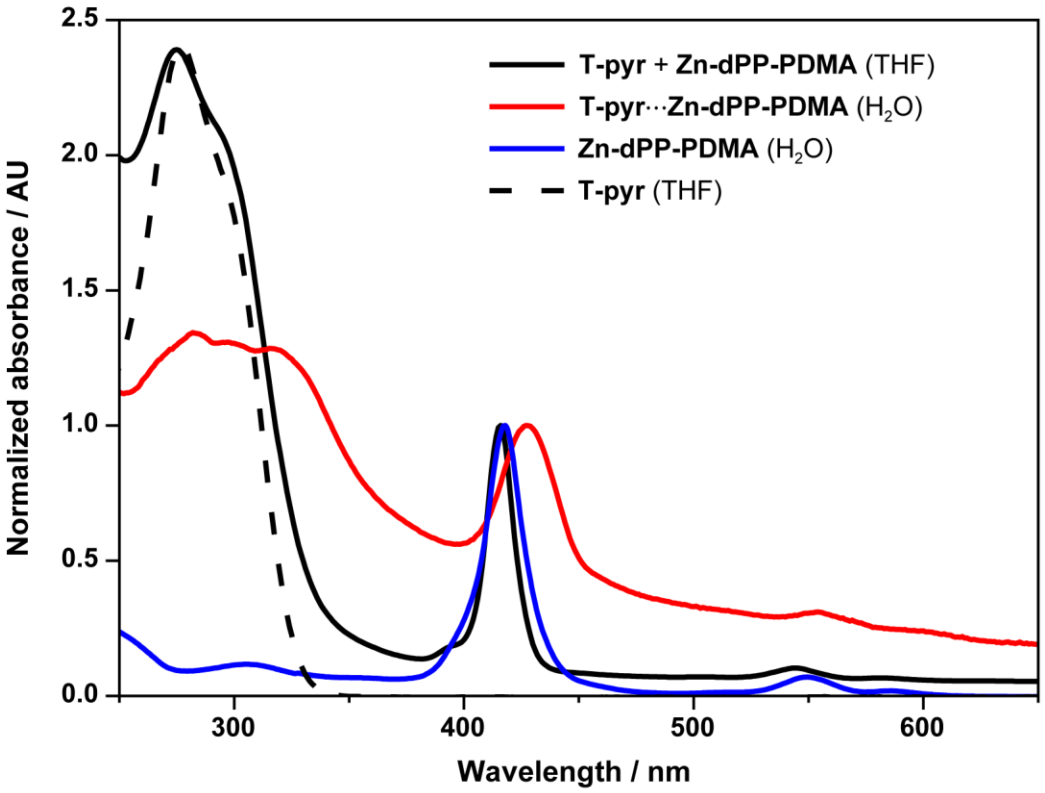

Figure S1. Full steady-state UV-visible absorption spectra. Results have been normalized to the Soret Band peak in all cases.

Analysis of TEAS data

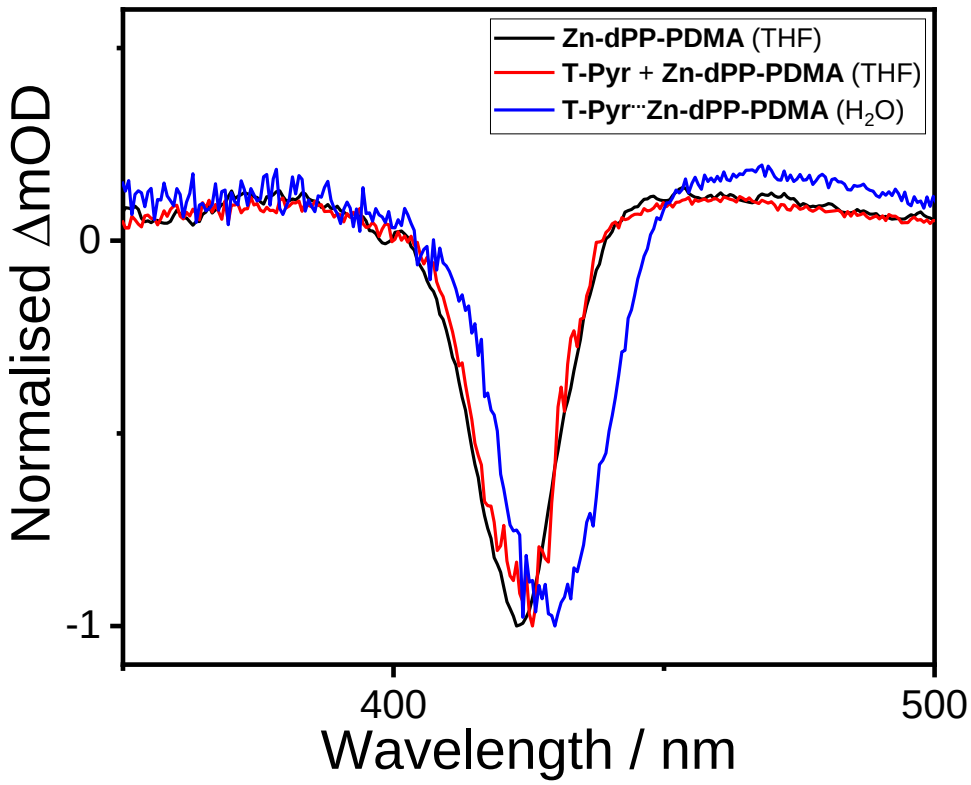

Figure S2. Transient absorption spectra at Dt = 1 ps for (black) **Zn-dPP-PDMA** in THF, (red) **T-Pyr+Zn-dPP-PDMA** in THF and (blue) **T-pyr···Zn-dPP-PDMA** in H_2O. Results have been normalized to the ground state bleach in all cases to highlight the red-shift for the templated assembly in water.

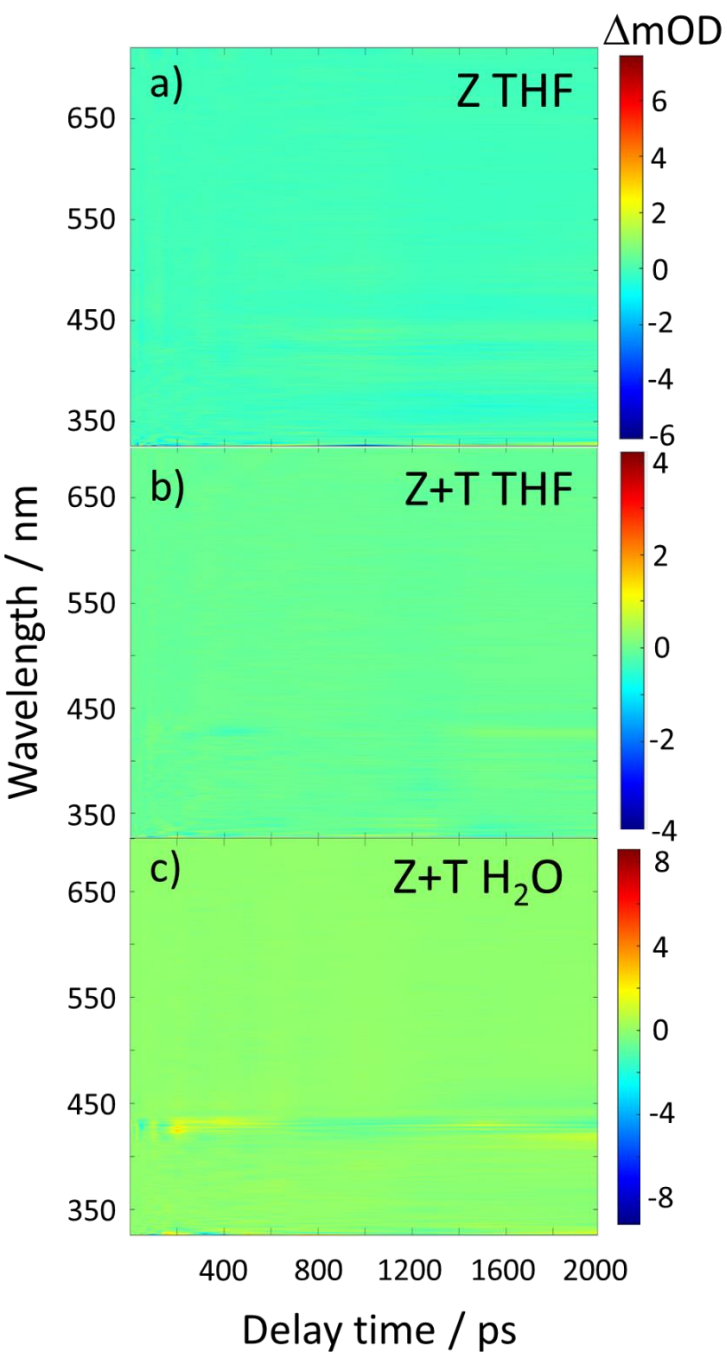

Figure S3. Residual from global fit analysis of TEAS data calculated as the fit of the data, minus the raw data for a) **Zn-dPP-PDMA** in THF, b) **T-pyr + Zn-dPP-PDMA** in THF and c) **T-pyr···Zn-dPP-PDMA** in H_2O. All fits show a deviation from the data of < 6%.

Calculated Molecular Orbitals and Transitions of Zn-dPP

The molecular orbitals of **Zn-dPP** that are involved in the transitions corresponding to the Soret band were calculated using the Turbomole[7-9] software package, using density functional theory, with the B-P86 functional,[10,11] the def2-SV(P) basis set,[12] the 'M4' quadrature scheme,[13] and employing the resolution of identity and multipole accelerated resolution of identify approximations with default auxiliary basis sets.[14,15] The orbitals are plotted in Figure S4 with details in Table S1.

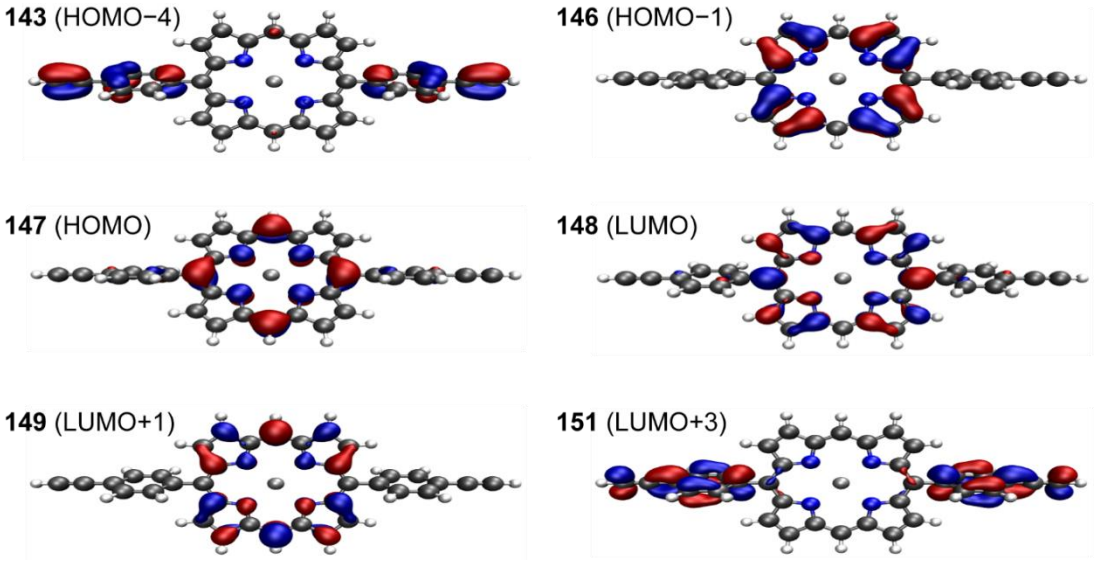

Figure S4. Representations of the calculated frontier molecular orbitals involved in the Soret band transition of **Zn-dPP**, with orbital numberings corresponding to those in Table S1.

Table S1. Character of transitions involved in the Soret band for **Zn-dPP.**

	Molecular orbital contribution and character			
Calculated transition wavelength / nm	**Initial orbital**	**Final orbital**	**Contribution / %**	**Oscillator strength**
434	143 (π)	148 (π*)	72%	0.5
	146 (π)	149(π*)	19%	

	147 (π)	151 (π*)	72%	
417	146 (π)	149(π*)	11%	0.4
	143 (π)	148 (π*)	11%	

References

(1) Quan, W.-D.; Pitto-Barry, A.; Baker, L. A.; Stulz, E.; Napier, R.; O'Reilly, R. K.; Stavros, V. G.; Chem. Commun., 2016, 52,1938–1941

(2) Hoffmann, M.; Kärnbratt, J.; Chang, M.-H.; Herz, L. M.; Albinsson, B.; Anderson, H. L.; Angew. Chem. Int. Ed., 2008, 47, 4993–4996

(3) Patterson, J. P.; Sanchez, A. M.; Petzetakis, N.; Smart, T. P.; Epps, T. H.; Portman, I.; Wilson, N. R.; O'Reilly, R. K.; Soft Matter, 2012, 8, 3322–3328

(4) Woolley, J. M.; Staniforth, M.; Horbury, M. D.; Richings, G. W.; Wills, M.; Stavros, V. G.; J. Phys. Chem. Lett. 2018, 9, 3043-3048.

(5) Grubb, M. P.; Orr-Ewing, A. J.; Ashfold, M. N. R. Rev. Sci. Instrum. 2014, 85, 064104.

(6) Snellenburg, J. J.; Laptenok, S. P.; Seger,R.; Mullen, K. M.; van Stokkum, I. H. M.; J. Stat. Softw. 2012, 49, 1–22.

(7) TURBOMOLE V6.2 2010, a development of University of Karlsruhe and Forschungszentrum Karlsruhe GmbH, 1989-2007, TURBOMOLE GmbH, since 2007; available from http://www.turbomole.com.

(8) Von Arnim, M.; Ahlrichs, R. J. Comput. Chem. 1998, 19, 1746-1757.

(9) Ahlrichs, R.; Bar, M.; Haser, M.; Horn, H.; Kolmel, C. Chem. Phys. Lett. 1989, 162, 165-169

(10) Becke, A. D. Phys. Rev. A 1988, 38, 3098-3100.

(11) Perdew, J. P. Phys. Rev. B 1986, 33, 8822-8824.

(12) Weigend, F.; Ahlrichs, R. Phys. Chem. Chem. Phys. 2005, 7, 3297-3305.

(13) Treutler, O.; Ahlrichs, R. J. Chem. Phys. 1995, 102, 346-354.

(14) Eshuis, H., Yarkony, J., & Furche, F. J. Chem. Phys., 2010. 132, 234114.

(15) Sierka, M., Hogekamp, A., & Ahlrichs, R. J. Chem. Phys. 2003 118, 9136–9148.